Solid State Communications 218 (2015) 1–5

Contents lists available at ScienceDirect

Solid State Communications

journal homepage: www.elsevier.com/locate/ssc

Phase stability and elastic properties of $CuGaSe_2$ under high pressure

Prayoonsak Pluengphon [a,*], Thiti Bovornratanaraks [b,c]

[a] Division of Physical Science, Faculty of Science and Technology, Huachiew Chalermprakiet University, Samutprakarn 10540, Thailand
[b] Extreme Conditions Physics Research Laboratory, Department of Physics, Faculty of Science, Chulalongkorn University, Bangkok 10330, Thailand
[c] ThEP Center, CHE, 328 Si-Ayuttaya Road, Bangkok 10400, Thailand

ARTICLE INFO

Article history:
Received 11 April 2015
Received in revised form
24 May 2015
Accepted 27 May 2015
Communicated by A.H. MacDonald
Available online 11 June 2015

Keywords:
A. $CuGaSe_2$
C. Phase stability
D. Elastic properties
D. High pressure

ABSTRACT

We report stability of high pressure phases and elastic properties in $CuGaSe_2$, especially in cubic and orthorhombic phases. The distorted structures from $Fm\bar{3}m$ and *Cmcm* consist of *Pmmn*, *P21/m*, *Amm2* and *P4/mmm* were observed. Cu and Ga sites in $Fm\bar{3}m$ and *Cmcm* can distinguish in the lower symmetry space groups which are *P4/mmm* and *Amm2*, respectively. The enthalpy differences of an interested structure are compared in the pressure range 0–100 GPa. The phonon dispersion relation of $CuGaSe_2$ was studied, and found that the *P4/mmm* and *Amm2* space groups give stability of phonon vibration modes. Moreover, we observe chemical bonds and elastic properties of $CuGaSe_2$ at high-pressure conditions. Elastic constants indicate mechanical stability of $CuGaSe_2$ in *P4/mmm* and *Amm2* phases. Although $CuGaSe_2$ has become nonsemiconductor material in the *P4/mmm* and *Amm2* phases, the strong of covalent bonds and sharing electrons are still increased by high pressure effect.

© 2015 Elsevier Ltd. All rights reserved.

1. Introduction

Nowadays, one major problem of the world is an energy crisis, and solar energy is a vivid choice of solutions. The efficiencies of solar cells highly depend on the physical and optical properties of semiconducting materials in multilayer structures. The I–III–VI_2 ternary compounds, such as $CuInSe_2$ (CIS) and $CuGaSe_2$ (CGS), have recently emerged as a very promising material for photovoltaic solar-energy application [1–4]. Under the conditions of high-pressure and temperature, many semiconductors and their alloys undergo a solid-solid transition from a disordered to an ordered structure because the different constituent atoms tend to occupy special sites in the lattice [5,6]. The high-pressure effect is a powerful modern tool for changing structures and properties of material because bond lengths and lattice parameters in unit cell were changed by the external forces. At ambient pressure (0 GPa), a stable structure of $CuAlSe_2$, $CuInSe_2$ and $CuGaSe_2$ is a chalcopyrite phase with space group $I\bar{4}2d$. By using energy dispersive x-rays diffraction (XRD) with synchrotron radiation and Merill–Bassett diamond anvil cell, Tinoco et al. [7,8] found that the 1st phase transition from chalcopyrite phase to NaCl-like cubic phase ($Fm\bar{3}m$) in $CuInSe_2$ occurs at 7.6 GPa, in which the volume reduction at transition point is about 10%. Gonzalez and Rincon [9] studied the optical absorption and phase transitions in Cu-III–VI_2 compound under hydrostatic pressure up to 20 GPa. They found that the $I\bar{4}2d \rightarrow Fm\bar{3}m$ phase transition of $CuGaSe_2$ occurs at 13.6 GPa. Later, Bovornratanaraks et al. [10] studied structures of $CuInSe_2$ up to 53 GPa using angle-dispersive x-ray powder diffraction techniques. The XRD result suggested that the $Fm\bar{3}m$ space group is completely transformed to the *Cmcm* phase at 43.9 GPa. The experiments suggested the atomic positions of cations (I–III) in $Fm\bar{3}m$ and *Cmcm* are the same atomic positions. *Ab initio* calculations [11,12] compared the free energies of space groups ($I\bar{4}2d$, $Fm\bar{3}m$ and *Cmcm*) from the experiments suggestion. The enthalpy comparisons showed that the order of phase transitions both $CuInSe_2$ and $CuGaSe_2$ are $I\bar{4}2d \rightarrow Fm\bar{3}m \rightarrow Cmcm$. They suggested that the high pressure phases of CIS and CGS are nonsemiconductor phases because band gaps in $Fm\bar{3}m$ and *Cmcm* are vanished by high pressure effect.

In previous works, band structures, density of states and free energies comparisons of $CuGaSe_2$ under high pressure were intensively studied. However, stability of phases, lattice vibration modes, chemical bonds and elastic properties are still incomplete. In this work, the phase stability of $CuGaSe_2$ under high pressure has been studied using the *ab initio* method which based on density functional theory (DFT). The distorted structures obtained from $Fm\bar{3}m$ and *Cmcm* consist of *Pmmn*, *P21/m*, *Amm2* and *P4/mmm* are analyzed. Mechanical stability of high-pressure phases was investigated by elastic parameters. Type of bonding in CGS was introduced by studying the electron density difference.

2. Calculation details

In this work, *ab initio* calculations were performed using self-consistent field method (SCF) as implemented in Cambridge Serial

* Corresponding author.
E-mail address: prayoonsak@gmail.com (P. Pluengphon).

http://dx.doi.org/10.1016/j.ssc.2015.05.019
0038-1098/© 2015 Elsevier Ltd. All rights reserved.

Total Energy Package (CASTEP) code [13,14]. In SCF loops, the ground state properties of a unit cell are obtained from the solution of Kohn–Sham equations. The generalized-gradient approximation (GGA) functional of Perdew–Burke–Ernzerhof (PBE) [15,16] was adopted for the exchange-correlation term in Kohn–Sham equations. The ultrasoft pseudopotentials [17] were used, and the cutoff energy which is the maximum energy of plane wave basis set was set to 500 eV for all calculations. Monkhorst–Pack grid sizes [18] for SCF calculations are $5\times5\times6$ for chalcopyrite phase, $6\times6\times6$ for cubic and orthorhombic structures. The condition of k point is $1/k\approx0.035$. The Brodyden–Fletcher–Goldfarb–Shanno (BFGS) [19] minimization scheme was used in geometry optimization for each volume. Forces and pressure tensors on geometry optimized structures were controlled by Hellmann–Feynman theorem [20]. The BFGS optimization was considered to be completed when the total energy difference was less than 5×10^{-7} eV/atom, Hellman–Feynman forces were less than 0.01 eV/Å, the maximum ionic displacement within 0.0005 Å, and all of the stress components within 0.02 GPa. The minimum free energies at 0 K of high-pressure structures were considered from the enthalpy differences, which the enthalpy in each structure obtained from the relation $H=E+PV$. Phonon dispersion calculations were observed using a finite displacement method [21] with super cell size $3\times3\times3$. The elastic constants, the average isotropic bulk modulus (B) and shear modulus (G) obtained from Voigt–Reuss–Hill (VRH) method [22,23] which bases on the single crystal elastic constants.

3. Results and discussion

For analyzing the crystal structures of $CuGaSe_2$ obtained from the CASTEP code, the optimized structures from GGA-PBE and LDA-CAPZ are compared to the previous studies in Table 1. It was found that lattice parameters and volume cells calculated from GGA-PBE functional are larger than the parameters from experiment, while the LDA results are lower than experiment and GGA-PBE. Bulk modulus at 0 GPa (B_0) can be obtained from fitting equation of states of energy (E) and volume (V). The bulk modulus from DFT calculations depend on using the correlation functional and equation of state. The calculated result from LDA-PW by fitting to a third-order Vinet equation of state [3] is 84.5 GPa, while the FP-LMTO+LDA result fitting from Birch equation of state [25] is 79.97 GPa, and GGA-PBE (in VASP) result fitting from Murnaghan equation of state in Ref. [12] is 57.7 GPa. The present results fitting to the third order of Birch–Murnaghan equation of state are 64.0 (GGA-PBE) and 58.0 GPa (LDA). We think that the different bulk modulus from available calculations is due to the varying of the fitting equation of states. We select the GGA-PBE functional for calculations the high-pressure structures because it gave the better lattice parameters and bulk modulus than LDA, when compare with the experiment [26]. Atomic coordinates at 0 GPa of Cu, Ga and Se are (0, 0, 0), (0, 0, 0.5) and (0.244, 0.25, 0.125), respectively. In previous experiments [7–10], it has been suggested that $Fm\bar{3}m$ and *Cmcm* structures are the thermodynamically stable phases of $CuInSe_2$ and $CuGaSe_2$ beyond the ambient phase ($I\bar{4}2d$), and atomic positions of Cu and Ga are not distinguish both $Fm\bar{3}m$ and *Cmcm*. In this calculation, we imposed the lower symmetry space groups on $Fm\bar{3}m$ and *Cmcm* structures which the Cu and Ga atomic positions are distinguish, so that it can be optimized by geometry optimization. The impose symmetry obtained from $Fm\bar{3}m$ is *P4/mmm*, while *Amm2* is the impose symmetry of *Cmcm*. We observed another 2 structures which are *P21/m* and *Pmmn*. The atomic positions of Cu, Ga and Se sites in $I\bar{4}2d$, *P4/mmm*, *Amm2*, *P21/m* and *Pmmn* are shown in Table 2. The enthalpy differences in all structures at 0 K are compared with *P4/mmm* as shown in Fig. 1. We found that the high pressure structures of in $CuGaSe_2$, which gave the minimum free energies, are $I\bar{4}2d$ at 0–12 GPa, *P21/m* at 12–52 GPa and *Amm2* at 52–100 GPa, respectively. Structures of $I\bar{4}2d$, *P4/mmm*, *P21/m and Amm2* are shown in Fig. 2(a), (b), (c) and (d), respectively. Although *P21/m* gave the minimum enthalpy in the pressure range of 12–52 GPa, we found that atomic positions in the *P21/m* and *Amm2* are approached to the *P4/mmm* space groups as shown in Fig. 2(b). The enthalpy differences (12–52 GPa) of *P21/m* and *Amm2* compared with *P4/mmm* are lower than 0.03 eV. This value occurred because the symmetry of *P4/mmm* is higher than *P21/m* and *Amm2*. And then, we observe the phonon dispersions of $I\bar{4}2d$ (0 GPa), *P4/mmm* (30 GPa) and *Amm2* (80 GPa) as shown in Fig. 3. The phonon dispersions show all positive vibration modes in $I\bar{4}2d$ at 0 GPa, *P4/mmm* at 30 GPa and *Amm2* at 80 GPa. Therefore, we can conclude that the stable phase of $CuGaSe_2$ (12–52 GPa) which has the higher symmetry than *P21/m* is *P4/mmm*. The *P4/mmm* space group obtained from $Fm\bar{3}m$ that can distinguish Cu and In sites in the primitive cell. These results confirm the experiments and calculations studies [10–12], but we can distinguish the Cu and Ga sites in $Fm\bar{3}m$ and *Cmcm* to the *P4/mmm* and *Amm2*, respectively. At the transition pressure 52 GPa (*P4/mmm* to *Amm2*), the equilibrium point in cubic phase (*P4/mmm*) was pressed, and changed to orthorhombic space group (*Amm2*) as shown in Fig. 2(c). The Cu–Se planes shift from Ga–Se planes that same as the CIS [11] and CIGS [27] phase transitions. The phonon density of states (PDOS) in $I\bar{4}2d$ (0 GPa), (30 GPa) and *Amm2* (80 GPa) were compared in Fig. 3(d). Peak of PDOS at 8.5 THz ($I\bar{4}2d$0 GPa) shift to 9.5 THz (*P4/mmm* 30 GPa) and 11.2 THz (*Amm2* 80 GPa). The maximum frequencies and peaks

Table 1
Comparison of lattice parameters ($a=b$ and c) and bulk modulus at 0 GPa (B_0) in chalcopyrite structure of $CuGaSe_2$ with previous studies.

a (Å)	c (Å)	c/a	B_0 (GPa)	Method	Ref.
5.628	11.157	1.982	64.0	GGA-PBE (in CASTEP)	This work
5.498	10.937	1.989	58.0	LDA-CAPZ (in CASTEP)	This work
5.435	10.712	1.971	84.5	LDA-PW	[3]
5.681	11.209	1.973	57.7	GGA-PBE (in VASP)	[12]
5.542	10.840	1.957	57.84	FP-LAPW+LDA	[24]
5.544	10.717	1.933	79.97	FP-LMTO+LDA	[25]
5.596	11.003	1.966	71	Experiment	[26]

Table 2
The atomic positions of Cu, Ga and Se in $I\bar{4}2d$, *P4/mmm*, *Amm2*, *P21/m* and *Pmmn* space groups at 0, 40 and 80 GPa, angles $\alpha=\beta=\gamma=90^{\circ}$ (except in *Amm2* at 80 GPa $\gamma=85.2^{\circ}$).

Space group	Cu site	Ga site	Se site	a (Å)	b (Å)	c (Å)	H–$H_{P4/mmm}$ (eV)
$I\bar{4}2d$ at 0 GPa	(0,0,0)	(0,0,0.5)	(0.244,0.25,0.125)	5.628	5.628	11.157	−1.100
P4/mmm at 40 GPa	(0,0,0.5)	(0.5,0.5,0)	(0,0,0)	3.418	3.418	4.782	0.000
P21/m at 40 GPa	(0.25,0.25,0)	(0.25,0.75,0.50)	(0.75,0.25,0)	4.840	4.840	4.767	−0.020
Pmmn at 40 GPa	(0,0,0.900)	(0,0.5,0.371)	(0,0,0.441)	4.444	4.748	5.233	0.067
Amm2 at 40 GPa	(0.5,0,0.258)	(0,0,0.740)	(0,0,0.243)	4.779	4.835	4.837	−0.002
Amm2 at 80 GPa	(0.5,0,0.369)	(0,0,0.629)	(0,0,0.168)	3.383	3.383	4.217	−0.200

of PDOS are extended under pressure increasing. This indicates the hardening of phonon vibration modes under high pressure.

From the optimized structures, the elastic constants (C_{ij}) can be calculated from a stress–strain method. Elastic constants of solids can provide the resistance of material in each direction due to the effect from external forces. The elastic properties of a material are essential to understand the chemical bond in material because type of bond relates with the hardness, stress and strain of material. A study of elastic properties in each stable structure is significant to understand the mechanical properties of $CuGaSe_2$ under high pressure. We compare the elastic properties at 0 GPa with previous works [3,25] as shown in Table 3. C_{11}, C_{12} and C_{13} from GGA-PBE are lower than other calculations, while C_{33}, C_{44} and C_{66} are in good agreement. However, B_0 obtained from GGA-PBE in this work is 64 GPa, while the experiment [26] reported as 71 GPa. The elastic stiffness tensor of $I\bar{4}2d$ at 0 GPa is satisfy the conditions of $C_{11}, C_{33}, C_{44}, C_{66} > 0, C_{11} > |C_{12}|, C_{11}C_{33} > C_{13}^2, (C_{11} + C_{12})C_{33} > 2C_{13}^2$, which are Born stability criteria in chalcopyrite lattice [3,12]. Moreover, the elastic parameters in Table 3 satisfy Born stability criteria in all structures [23,28]. These indicate that the structures of $CuGaSe_2$ are mechanically stable phases under high pressure. Under high-pressure, we can see that C_{11} is more sensitive with pressure increasing than C_{12} and C_{44} because C_{11} indicates the elasticity in length while C_{12} and C_{44} relate with shear constant and elasticity in shape. From elastic constants, bulk modulus (B) and shear modulus (G) of polycrystalline can be obtained from VRH approximation. The critical B/G ratio of 1.75 separates type of ductile (> 1.75) and brittle (< 1.75) materials, which was introduced by Pugh [29]. However, Frantsevich et al. [30] suggested another critical ratio of $B/G = 2.67$. The B/G ratios in Table 3 indicate that CGS in *P4/mmm* and *Amm2* are ductile material. The bulk modulus, and elastic constant and B/G ratio calculated from VRH method were widely used to classify type of phase in compounds such as $MgCu_2$ [31], $HgGa_2Se_4$ [32], $CdGa_2Se_4$ [33], $HgGa_2Se_4$ [34] and $HgGa_2S_4$ [35]. Bulk modulus, C_{11}, and B/G ratio of $CuGaSe_2$ increase under high-pressure which related with the defect-chalcopyrite compounds ($HgGa_2Se_4$ and $HgGa_2S_4$) [32,35].

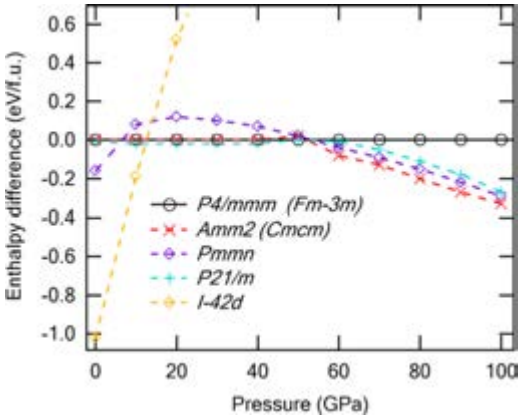

Fig. 1. The enthalpy differences at 0 K (compared with *P4/mmm*) of the possible space groups in $CuGaSe_2$ under pressure.

In addition, we also analyze the electron density difference as shown in Fig. 4. There are strong covalent bonds of Cu–Se and In–Se, and the red zone shows the sharing electrons which highly increase in *Amm2*. The blue zone shows that the electron density at Cu sites are decreased when compare with an isolated Cu atom. This indicates that the sharing electrons in chemical bonding mainly transform from Cu sites. The previous work [12] showed that band gap of $CuGaSe_2$ is vanished as the first phase transition ($I\bar{4}2d \rightarrow Fm\bar{3}m$), which band structures reported in Ref. [12]. Although $CuGaSe_2$ became nonsemiconductor in II and III phases, the strong of covalent bonds are increasing by high-pressure effect.

4. Conclusions

Ab initio calculations based on DFT were performed for studying phase stability and mechanical properties of CGS at high

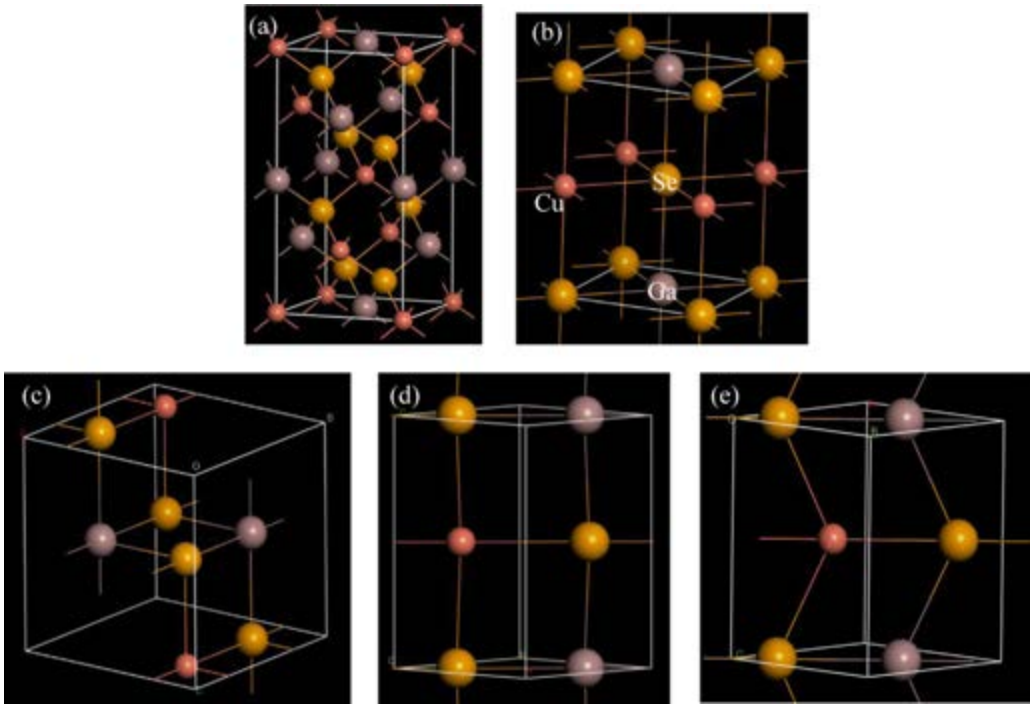

Fig. 2. Comparisons the optimized structures of $CuGaSe_2$ at high pressures. (a) $I\bar{4}2d$ at 0 GPa, (b) *P4/mmm* at 40 GPa, (c) *P21/m* at 40 GPa, (d) *Amm2* at 40 GPa and (e) *Amm2* at 80 GPa.

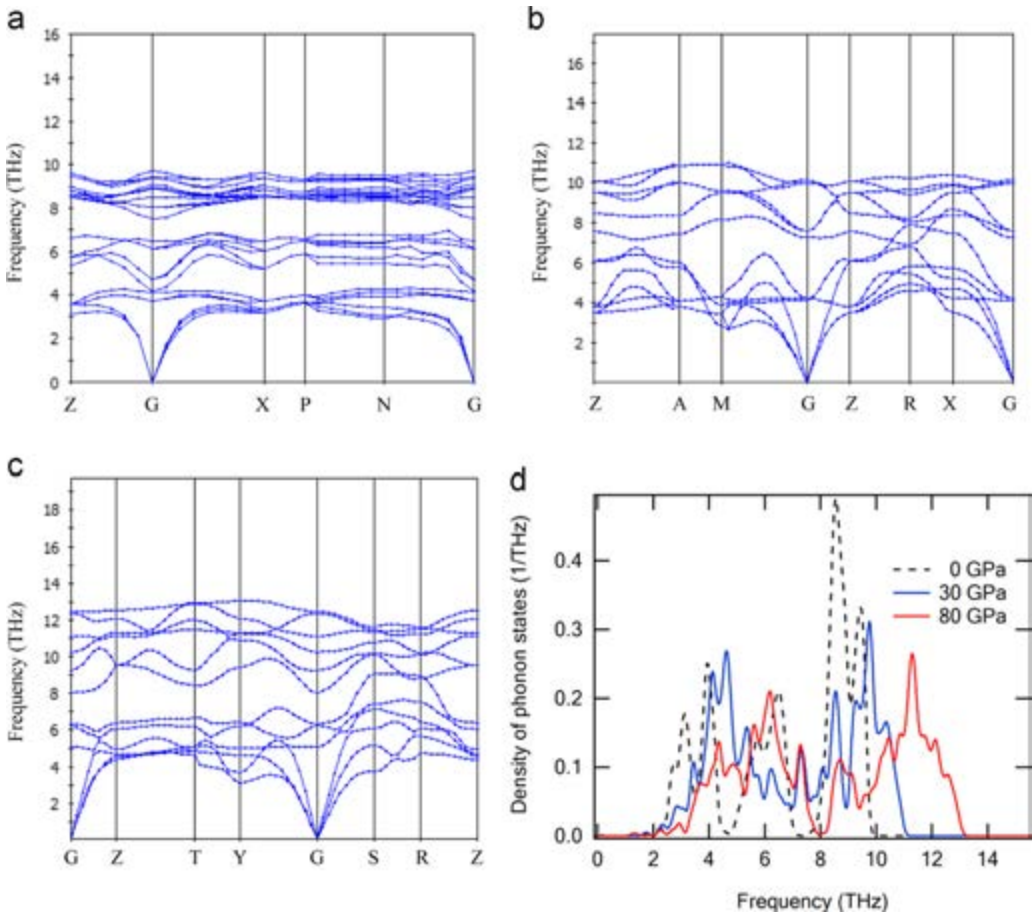

Fig. 3. Phonon dispersion and density of states of $CuGaSe_2$ under high pressure (a) $I\bar{4}2d$at 0 GPa, (b) *P4/mmm* at 30 GPa, (c) *Amm2* at 80 GPa and (d) phonon density of states.

Table 3
Elastic parameters in a unit GPa of $CuGaSe_2$ in the phases of $I\bar{4}2d$ (0 GPa), *P4/mmm* (30, 40 and 50 GPa) and *Amm2* (60, 80 and 100 GPa).

Phase	*P* (GPa)	C_{11}	C_{12}	C_{13}	C_{23}	C_{22}	C_{33}	C_{44}	C_{55}	C_{66}	*B*	*G*	*B*/*G*	Ref.
$I\bar{4}2d$	0	86	52	49	49	86	108	47	47	41	64	33	1.94	This work
		112.2	66.4	68.1	68.1	112.2	113	48.4	48.4	48.5	84.5	–	–	[3]
		105.65	63.29	63.03	63.03	105.65	106.03	47.38	47.38	46.69	62.79	26.95	2.33	[25]
P4/mmm	30	290	202	114	114	290	416	46	46	133	206	72	2.86	This work
	40	332	244	120	120	332	514	45	45	157	238	80	2.98	
	50	399	303	126	126	399	609	44	44	183	279	88	3.17	
Amm2	60	415	158	341	171	625	435	53	87	85	312	83	3.76	This work
	80	504	167	391	172	766	446	38	95	89	352	88	4.00	
	100	638	170	493	259	894	584	11	128	95	440	83	5.30	

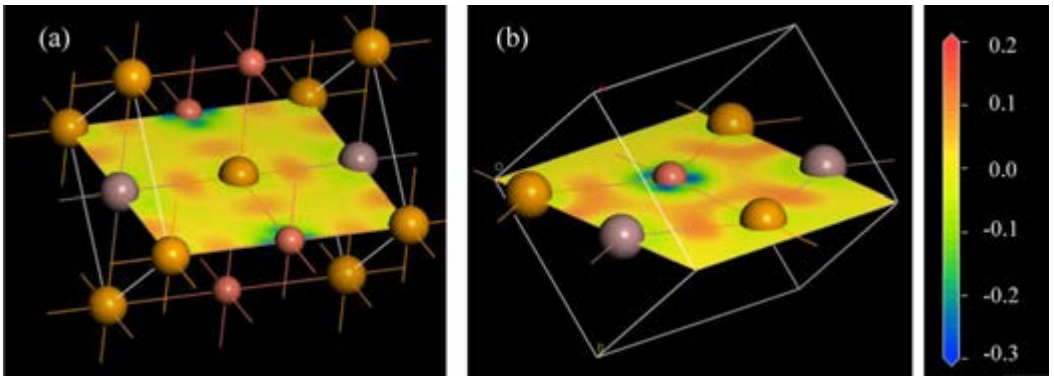

Fig. 4. Electron density difference of (a) *P4/mmm* at 30 GPa and (b) *Amm2* at 80 GPa. (For interpretation of the references to color in this figure, the reader is referred to the web version of this article.)

pressure. It was found that the impose symmetry obtained from $Fm\bar{3}m$ is *P4/mmm*, while *Amm2* is the impose symmetry of *Cmcm*. Cu and Ga sites in a CGS unit cell can distinguish in the *P4/mmm* and *Cmcm*. The phonon dispersions show all positive vibration modes in *P4/mmm* at 30 GPa and *Amm2* at 80 GPa. In *P4/mmm*–*Cmcm* phase transition, the Cu–Se planes shift from Ga–Se planes that same as the CIS and CIGS phase transitions. The maximum frequencies and peaks of PDOS are extended under pressure increasing, which indicate the hardening of phonon vibration modes under high pressure. In elastic parameters, the mechanical stability of the $CuGaSe_2$ structures are satisfy the elastic constants conditions [23,28], which indicate that the high pressure structures of $CuGaSe_2$ are mechanically stable phases. The *B*/*G* ratios in table II indicate that CGS in *P4/mmm* and *Amm2* are ductile material. In addition, the chemical bond was analyzed by the contour plot of the density difference. The sharing electrons in chemical bonding mainly transform from Cu sites. The strong of covalent bonds in CGS are increasing by high-pressure effect.

Acknowledgments

P. Pluengphon would like to thank the financial support from Faculty of Science and Technology, Huachiew Chalermprakiet University. T. Bovornratanaraks acknowledges financial support from Asahi Glass Foundation, National Research Council of Thailand and Thailand Research Fund Contract number DBG5280002. Computing facilities are supported by The National Research University Project of CHE and the Ratchadaphiseksomphot Endowment Fund (FW657B).

References

[1] M. Turowski, G. Margaritondo, M.K. Kelly, R.D. Tomlinson, Phys. Rev. B 31 (1985) 1022.
[2] C. Persson, Y. Zhao, S. Lany, A. Zunger, Phys. Rev. B 72 (2005) 035211.
[3] C. Parlak, R. Eryigit, Phys. Rev. B 73 (2006) 245217.
[4] F.Y. Liu, J. Yang, J.L. Zhou, Y.Q. Lai, M. Jia, J. Li, Y.X. Liu, Thin Solid Films 520 (2012) 2781.
[5] A. Zunger, Appl. Phys. Lett. 50 (1987) 164.
[6] C. Rincon, Phys. Rev. B 45 (1992) 12716.
[7] T. Tinoco, A. Polian, D. Gomez, J.P. Itie, Phys. Status Solidi (b) 198 (1996) 433.
[8] T. Tinoco, J.P. Itié, A. Polian, A.S. Miguel, E. Moya, P. Grima, J. Gonzalez, F. Gonzalez, J. Phys. IV 4 (1994) C9.
[9] J. Gonzalez, C. Rincon, J. Phys. Chem. Solids 51 (1990) 1093.
[10] T. Bovornratanaraks, V. Saengsuwan, K. Yoodee, M.I. McMahon, C. Hejny, D. Ruffolo, J. Phys.: Condens. Matter 22 (2010) 355801.
[11] P. Pluengphon, T. Bovornratanaraks, S. Vannarat, K. Yoodee, D. Ruffolo, U. Pinsook, Solid State Commun. 152 (2012) 775.
[12] H. Xue, F. Tang, W. Lu, Y. Feng, Z. Wang, Y. Wang, Comput. Mater. Sci. 67 (2013) 21.
[13] M.C. Payne, M.P. Teter, D.C. Allan, T.A. Arias, D. Joannopoulos, Rev. Mod. Phys. 64 (1992) 1045.
[14] M.D. Segall, P.L.D. Lindan, M.J. Probert, C.J. Pickard, P.J. Hasnip, S.J. Clark, M. C. Payne, J. Phys.: Condens. Matter 14 (2002) 2717.
[15] J.P. Perdew, J.A. Chevary, S.H. Vosko, K.A. Jackson, M.R. Pederson, D.J. Singh, C. Fiolhais, Phys. Rev. B 46 (1992) 6671.
[16] J.P. Perdew, K. Burke, M. Ernzerhof, Phys. Rev. Lett. **77** (1996) 3865.
[17] D. Vanderbilt, Phys. Rev. B 41 (1990) 7892.
[18] H.J. Monkhorst, J.D. Pack, Phys. Rev. B 13 (1976) 5188.
[19] B.G. Pfommer, M. Cote, S.G. Louie, M.L. Cohen, J. Comput. Phys. 131 (1997) 233.
[20] R.P. Feynman, Phys. Rev 56 (4) (1939) 340.
[21] P. Giannozzi, S. de Gironcoli, P. Pavone, S. Baroni, Phys. Rev. B 43 (1991) 7231.
[22] R. Hill, Proc. Phys. Soc. A 65 (1952) 349.
[23] G.V. Sinko, N.A. Smirnov, J. Phys.: Condens. Matter 14 (2002) 6989.
[24] M. Belhadj, A. Tadjer, B. Abbar, Z. Bousahla, B. Bouhafs, H. Aourag, Phys. Status Solidi (b) 241 (2004) 2516.
[25] T. Bouguetaia, B. Abidri, B. Benbahi, et al., Surf. Rev. Lett. 19 (2012) 1250021.
[26] H. Neumann, Phys. Status Solidi (a) 96 (1986) K121.
[27] P. Pluengphon, T. Bovornratanaraks, S. Vannarat, U. Pinsook, J. Phys.: Condens. Matter 24 (2012) 095802.
[28] F. Mouhat, F. Coudert, Phys. Rev. B 90 (2014) 224104.
[29] S.F. Pugh, Philos. Mag. 45 (1953) 833.
[30] I.N. Frantsevich, F.F. Voronov, S.A. Bokuta, Elastic Constants and Elastic Moduli for Metals and Insulators Handbook, Naukova Dumka, Kiev (1983) 60–180.
[31] Y. Liu, W. Hu, D. Li, X. Zeng, C. Xu, X. Yang, Intermetallics 31 (2012) 257.
[32] O. Gomis, R. Vilaplana, F.J. Manjon, et al., J. Appl. Phys. 113 (2013) 073510.
[33] S.H. Ma, Z.Y. Jiao, X.Z. Zhang, J. Mater. Sci. 47 (2012) 3849.
[34] D. Errandonea, Kumar, S. Ravhi, F.J. Manjon, et al., J. Appl. Phys. 104 (2008) 063524.
[35] O. Gomis, D. Santamaria-Perez, R. Vilaplana, et al., J. Alloy. Compd. 583 (2014) 70.